Physical Biology

ACCEPTED MANUSCRIPT

Raman spectroscopy of osteosarcoma cells

To cite this article before publication: Mario D'Acunto *et al* 2018 *Phys. Biol.* in press https://doi.org/10.1088/1478-3975/aaefbf

Raman Spectroscopy of Osteosarcoma Cells

Mario D'Acunto[1,*], Luisa Trombi[2], Delfo D'Alessandro[2] and Serena Danti[3]

[1]Consiglio Nazionale delle Ricerche, Istituto di Biofisica, CNR-IBF, via Moruzzi 1, I-56124, Pisa, Italy
[2]Dept. of Surgical, Medical, Molecular Pathology, and Emergency Medicine, University of Pisa, via Savi 10, 56126 Pisa, Italy
[3]Dept. of Civil and Industrial Engineering, University of Pisa, Largo L. Lazzarino 2, 56122 Pisa, Italy

E-mail: mario.dacunto@pi.ibf.cnr.it

Abstract

Osteosarcoma is the most common primary malignant bone tumor. In the last years, several studies have demonstrated that the increase of Hydroxyapatite (HA) and Interleukin-6 (IL-6) syntheses compared to those expressed by normal osteoblasts could be used to detect the degree of malignancy of osteosarcoma cells. Conventional biochemical methods widely employed to evaluate bone cell differentiation, including normal and cancerous phenotypes, are time consuming and may require a large amount of cells. HA is a mineral form of calcium phosphate whose presence increases with maturation of osteosarcoma cells. Analogously, IL-6 is a fundamental cytokine whose production is highly increased in osteosarcoma cells. In this study, we employ Raman spectroscopy to the identification and discrimination of osteosarcoma cells from osteo-differentiated mesenchymal stromal cells (MSCs) by detecting the presence of HA and IL-6. However, while the identification of HA is facilitated by the characteristic peak at $960 cm^{-1}$, corresponding to symmetric stretching (*P-O*) mode, the quantification of IL-6 it is much more elusive, being its Raman signal characterized by cysteine, but also by phenylalanine, amide I II and III whose signals are common to other proteins. Supported by an accurate multivariate analysis, the results show that Raman spectroscopy is a high sensitivity technique dealing out a direct and quantitative measurement of specific mineralization levels of osteosarcoma cells. In turn, by exploiting the Surface-Enhanced Raman Scattering stimulated by internalized Gold Nanoshells (AuNSs) and combined with scanning probe microscopies, we were able to employ Raman spectroscopy to study subcellular components locally.

Keywords: Raman spectroscopy, Osteosarcoma, Scanning Probe Microscopy

1. Introduction

Raman scattering, also known as Raman effect, is the inelastic scattering of photons exerted by molecules which are excited to higher vibrational or rotational energy levels [1]. Raman spectroscopy is based on inelastic scattering of molecular systems when illuminated by monochromatic radiation. The Raman intensities depend on the scattering cross section of the light interacting with the object of interest, which are proportional to the polarizability of the object to be measured [2].

Raman spectroscopy owns the great advantage of subcellular observation [3-6]. Indeed, the observation of single cells bypasses the strongly absorption of infrared light by the extracellular matrix water content. Hence, the Raman spectroscopy can provide information on the molecular composition of single cells. This is particularly important in oncology as normal or tumor cells may have different molecular composition. The traditional limitations to current Raman spectroscopy, namely, the low efficiency of inelastic scattering, can be solved incorporating more powerful optical techniques, such as surface-enhanced Raman spectroscopy (SERS) or tip-enhanced Raman spectroscopy (TERS) [7-9]. SERS effects are generated by the enhancement of Raman scattering by molecules adsorbed on a rough metal surface or by nanostructures such as metal nanoparticles or plasmonic nanosystems.

The combination of Raman spectroscopy with some features of high-resolution scanning probe microscopy (SPM) has generated the TERS technique. TERS is a near-field spectroscopic technique, which detects simultaneously both the topography and the Raman spectrum with nanometer spatial resolution using a sharp SPM metal tip.

In this paper, we investigated the osteosarcoma cell (i.e., MG-63, human osteosarcoma cell line), against the osteoblast obtained by MSC osteogenic differentiation as the non-tumor counterpart.

MSCs play a fundamental role in bone formation as they own the capability of differentiation into osteoblasts, as well as other mesodermal cells, such as adipocytes, chondrocytes and tenocytes [10]. Osteoblasts are the bone matrix forming cells deputed to a proper maintenance of the skeleton through the secretion of mineral (particularly, HA) and organic bone matrix. Osteosarcoma is one the most cancer affecting bone tissue [11]. The exact origin of osteosarcoma cells is still unclear. Reported findings are prone to indicate dysfunctional MSCs of central importance to the genesis of this cancer [12].

MG-63 cells were chosen for this study since they are considered low malignancy grade osteosarcoma cells. In fact, although MG-63 cells were derived from cancer specimens, they have sometimes been used in place of normal osteoblasts (much more difficult to isolate and culture) for general studies in the biomaterials field [13]. Therefore, with respect to other osteosarcoma cell lines, such as SaOS-2 and HOS T85, MG-63 cells should represent a good model against which to test the sensitivity of our detecting method. Indeed, the grade of malignancy of a tumor cell may be a difficult parameter to precisely assess. The Raman spectroscopy can provide relevant insight to this and other questions, as it is able to give detailed information on the molecular texture of a cell. In this study, we focused the attention to HA and IL-6, due to evidenced increase of such components in MG-63 compared to normal osteoblast-like cells [14-15]. Apatites are calcium-phosphates with the general crystal cell unit $Ca_{10}(PO_4)_6X_2$. Among others, the apatite-substituting ions (X) found in bone and teeth are F, Cl, B, OH. Bone HA with general formula $(Ca_{10}(PO_4)_6(OH)_2$ and space group $P6_3/m$ has been extensively studied with Raman spectroscopy for its important role in biological systems and biomedical materials [16]. Vibrational spectroscopy can evidence the $(PO_4)^{3-}$ and OH^- ions that are the basic units of HA. The phosphate group is characterized by v_1 symmetric stretching (P-O) mode at 960cm^{-1}, v_2 bending (O-P-O) mode at 430-450cm^{-1}, v_3 antisymmetric stretching (P-O) mode at 1020-1080cm^{-1}, usually overlapping with proline v(C-C) component and v_4 bending (O-P-O) mode at 585-610cm^{-1} [17]. The biological environment where is immersed the HA can produce a very broad band usually of fluorescent nature, or non-fluorescent nature [18]. In vitro studies on normal osteoblast and osteosarcoma cell lines have shown distinct mineralization profiles, including extent of mineral deposits, which is higher in cancer cells, as well as slight differences in HA composition, being, for example, Cl and F substitutions in Cl-substituted HAs more frequent in normal than in cancer cells [19].

In a similar fashion to other ILs, IL-6 is a component of cytokines that are small proteins (Mw~5-20kDa) with a key role in cell signaling [20]. It has been demonstrated that IL-6 has a fundamental role in bone metastasis and cancer progression [15]. In fact, IL-6 has a strong pro-tumorigenic activity due to its multiple effects on bone metabolism and tumor cell proliferation. The role of IL-6 in human osteosarcoma is demonstrated by the observation of elevated serum levels of IL-6 in patients with bone metastasis. Raman spectra of IL-6 are rather complex and present still unknown features [21]. SERS measurements on IL-6 evidenced relevant intensity of the nitro moiety band of the between 1330 cm^{-1} and 1350 cm^{-1}, essentially coincident with amide III [22].

This study aims to demonstrate that the application of Raman spectroscopy, Raman imaging and SERS to investigate MSCs, osteoblasts and osteosarcoma cells gave us the possibility to identify the presence of HA (and correspondent mineralization rate) and/or IL-6 as a fingerprint of tumor transformation of MSCs.

Having a live imaging tool able to detect the presence of osteosarcoma cells in the margins after tumor removal would enable a precise resection (neither too low, nor too much extensive), which will ultimately result in higher survival and better quality of life of patients.

2. MATERIALS and METHODS

A. Cells culture

Normal, cancerous and mixed cells were cultured on glass slides, as follows:

i) Undifferentiated MSCs. MSCs were isolated from human bone marrow according to a previously reported method [23] and used at passage 2 to perform three culture strategies. MSCs were plated on glass slides inside Petri dishes at a density of 20,000 cells in DMEM-LG supplemented with 10% fetal bovine serum (FBS). The samples were cultured for 72 h, then fixed in 1% neutral buffered formalin for 10 min at 4°C.

ii) Osteo-differentiated MSCs. MSCs were plated on glass slides at 20,000 cells as above. After 24h the culture medium was replaced with osteogenic medium consisting of DMEM-LG, 10% FBS, 10 mM β-glycerophosphate, 50 µg/ml ascorbic acid and 10^{-7} M hydrocortisone. Osteogenic medium was renewed twice a week for 14 days in order to initiate early mineral matrix deposition, namely, expression of mature osteoblast phenotype. Finally, the samples were formalin fixed, as in *i*).

iii) Osteosarcoma cells. MG-63 (human osteosarcoma cell line ATCC® CRL-1427) cells were seeded on 6 slides at 10,000 cells in Eagle's Minimum Essential Medium (EMEM)

supplemented with 10% FBS and cultured for 72h; thereafter the samples were formalin fixed, as in *i*).

iv) Mixed cancer and normal cells. MSCs were plated on 6 glass slides inside Petri dishes at 10,000 cells in DMEM-LG supplemented with 10% FBS. In parallel, MG-63 cells were plated at passage 2 on 6-well tissue culture plate (50,000 cells/2 mL) in EMEM supplemented with 10% FBS. After 24 h, the MG-63 cells were harvested and seeded at 10,000 cells onto slides previously seeded with MSCs. After 72h the slides were formalin fixed, as in *i*).

In order to amplify the Raman signal exploiting SERS effect, osteo-differentiated MSCs and MG-63 cells were loaded with gold nanoshells (AuNSs) diluted 1:20 in the culture media 24h before the endpoint. The AuNSs used had nominal diameter of nearly 160nm (120nm SiO2 core +40nm gold shell) and were provided by Nanocomposix® (San Diego, USA) [24].
At each endpoint, all the samples were fixed in 1% (w/v) neutral buffered formalin for 10min at 4°C.

B. Raman spectroscopy

Raman spectra were recorded with a Thermo Fisher Scientific DXR2xi Raman microscope with the following experimental parameters: laser wavelength 532nm; power laser of 5-10mW; $400\text{-}3400\text{cm}^{-1}$ full range grating; 10×, 50× and 100× objectives; 25µm confocal pinhole; 5(FWHM) cm^{-1} spectral resolution. Integration time for acquiring a Raman spectrum was 1 sec and 10 scans for any spectrum. In order to identify the best experimental parameters, preliminary measurements were performed to optimize the signal-to-noise ratio, and minimize the sample fluorescence. The background-subtracted Raman spectra were normalized for the area under the curve for standardization of the Raman intensities. The samples did not undergo any kind of pre-treatment before Raman examination. In turn, to assess intra-sample variability, multiple measurements were carried out at different regions within the sample.

Topography of cells was recorded with an AFM operating in alternative contact. Identification of internalized AuNSs was performed with bright- and dark-field microscope aided by the combined use of AFM and EFM [25].

C. Signal Processing and Statistical methods

Classical Least Squares (CLS)

The CLS fitting procedure provides that at each point within the multidimensional spectral array, the CLS fitting method finds a linear combination of the reference component spectra with best fits the raw data.

Principal component analysis (PCA)

PCA is a multivariate technique acting in an unsupervised manner. PCA reduces the dimensionality of the data set by finding an alternative set of new coordinates representing the principal components. PCA was conducted over the Raman spectra data sets on the range (400-2000cm⁻¹), with the aim of comparing the spectral data in terms of similarities and differences. Scores was examined to see how similar spectra are clustered. Loadings was also plotted to find out which wavenumber contributed most to various PCs.

Linear Discriminate Analysis (LDA)

On the contrary, to PCA, LDA is a multivariate technique acting in a supervised manner, meaning that it is required an *a priori* knowledge of how many Raman peaks are under investigation and which samples correspond to each peak.

Omnic 9.0 software for pre-processing and background removal [26], and an *ad-hoc* code written in Matlab® [27] for managing spectral data and statistical data analysis were used.

3. RESULTS and DISCUSSION

The Raman spectroscopic study was first carried out on osteo-differentiated MSCs cells and osteosarcoma cells in order to be able to discriminate the different cellular populations. Hence, SERS study was performed on such different cell populations making use of AuNSs with the purpose to locally enhance the Raman signal.

The basic differences between osteo-differentiated MSCs and MG-63 cells, in absence of AuNSs, are evidenced by the Raman spectra displayed in Figure 1, and denoted by the arrows.
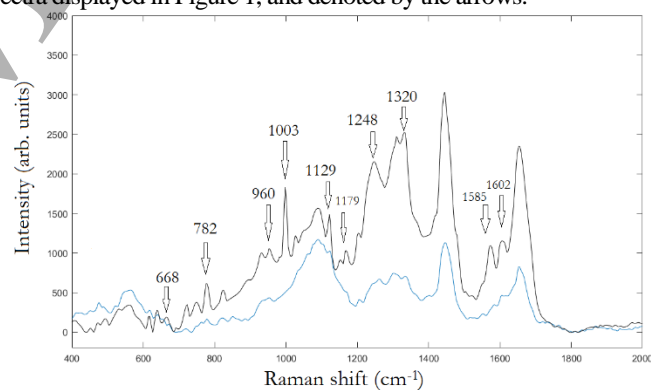

Figure 1. Averaged Raman spectra of osteo-differentiated MSCs (continue blue line), MG-63 cells.

The assignation of peaks is made after multivariate analysis and with the help of references [28], Table I. We first adopted PCA to extract the relevant information from the original data generating the new set of variables, i.e, the principal components covering >90% of total variance of the raw data. Subsequently LDA (a supervised method) was used to find similarities and differences between control group and osteosarcoma cells. The PCA requires an *i* by *j* matrix of Raman spectra (*i*=number of spectra, *j*= wave number) where highest spectral differences were associated to the principal components corresponding to, respectively, 668cm⁻¹, 782 cm⁻¹, 960cm⁻¹, 1003cm⁻

^{1}, 1129cm^{-1}, 1179 cm^{-1}, 1248 cm^{-1}, 1320cm^{-1}, 1585 cm^{-1} and 1602 cm^{-1}. The PCA was performed on the matrix 40×1600 of 40 averaged spectra including osteo-differentiated MSC and MG-63 populations from *ii*) and *iii*), respectively, see Materials and Methods section. Once PCA analysis made it possible to identify the most relevant differences between osteo-differentiated MSCs and MG-63 cells, and the, leaded by the main peaks previously identified, LDA was applied to find and classify putative eventual differences among the populations under investigation.

All the information about the possible differences in composition is contained within the first four principal components with a larger variance percentage %, PC1(48,4%), PC2(21,7%), PC3(13,0%) and PC4(7.8%), respectively.
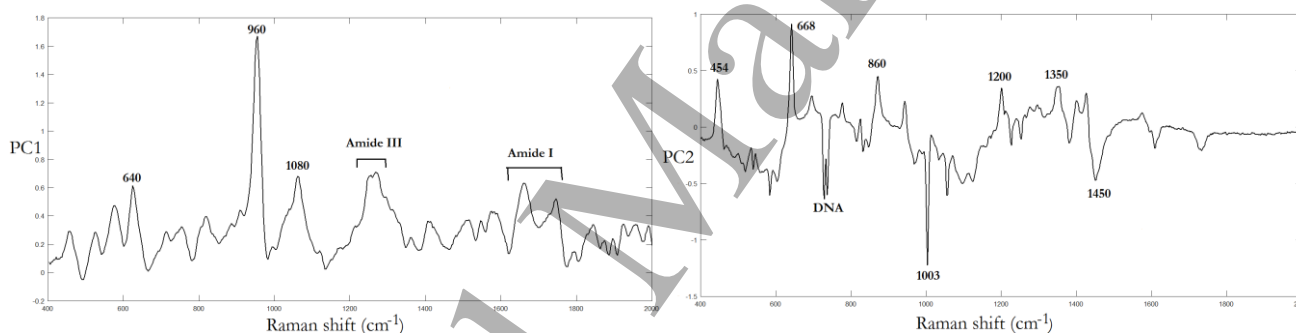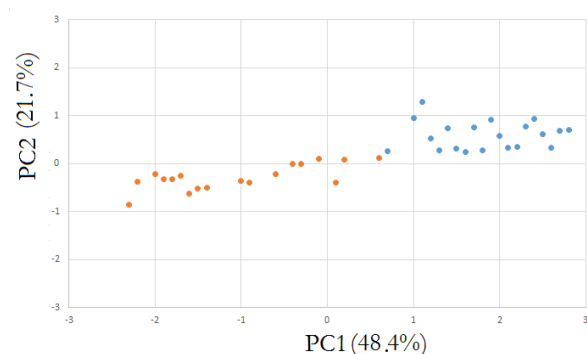

Figure 3. First two PCs (1,2) loadings plot.

Unlike osteo-differentiated MSCs, MG-63 cells showed the presence of HA as denoted by the peak of PO_4^{3-} ions at 960cm^{-1}. Other interesting changes in osteosarcoma cells are shown by the peaks at 1003cm^{-1} (as well as the peak at 1176cm^{-1}) generated

by Phenylalanine (Phe). Phe is an α-amino acid essential to form proteins, encoded by DNA. In humans, it may ultimately be metabolized into a range of different substances. However, elucidating the role of Phe in the maturation stage of osteosarcoma cells goes beyond the scope of this work.

The peak at 668cm^{-1} is assigned to cysteine being the symmetric stretching vibration of *C-S*. Cysteine is a semi-essential proteinogenic amino acid with the formula $HO_2CCH(NH_2)CH_2SH$. Cysteine is also a countersign of IL-6 [29-30]. Analogously, the other peaks marked in Figure 1 can be interpreted as a fingerprint of amide I, II, III (eventually connected to IL-6, as well as to other proteins).

The spectral region between 1200cm^{-1}-1350cm^{-1} can be assigned to amide III. Amide III band is composed principally of 40% *C-N*

Figure 2. Score plot in the PC1-PC2 plane. Blue dots represent MG-63 cells, while orange dots denote osteo-differentiated MSCs.

In order to verify whether any of the PCs can help to distinguish groups from normal and cancer cells, a two-sample *t*-test was applied on the scores for each of the 4 PCs, after checking any time the validity of the assumption of equality between the variances of the two groups by Fischer's test. The *t*-test confirms that for the 1-4PCs can be found the ability to discriminate between osteo-differentiated and MG-63 cells showing for the PCs the following *p*-values 0.027, 0.035, 0.041, 0.019, respectively.

The spectra of two first PC vectors are labeled in Figure 3 representing main peaks of each PC that can be related to Raman bands found in the 40 detected spectra.

stretch, 30% *N-H* bending. The peak at 1450 cm^{-1} is generated by CH_2 bending, in a special way, to CH_2 bending modes of methyl groups in malignant tissues due to deformation *C-H* bands [28]. The spectral band falling in the range 1550cm^{-1}-1600cm^{-1} can be assigned to Amide II, 60% *N-H* bending and 40% *C-N* stretch.

Further spectral regions allowed us to identify DNA components (asymmetric phosphate stretching vibration at ~1225 cm^{-1}) non-lipid substances, such as polymeric resins, substances that have long-chain structure, which have been used for sample preparation. In turn the nucleus area containing chromosome proteins, and cytoplasm enriched by proteinaceous substance (Amide I predominantly in α-helix conformation at ~1650cm^{-1}, and Amide II predominantly in β-sheet conformation at 1550cm^{-1}).The last peak marked by the arrow at 1660 cm^{-1} is the strongest component of amide I, 80% *C=O* stretch.

It should be noted that the relative intensities mainly correspond to the species concentration even though they can similarly be related to the orientation of the material or molecule with respect to the incoming laser polarization. This is the case of the strongest Amide I $v(C=O)$ component (1660cm^{-1}).

Raman shift (cm^{-1})	Band attribution
430-450	$v_2 PO_4^{3-}$ Strong band
584-590	$v_4 PO_4^{3-}$
668	$v(C-S)$ Cysteine
782	Ring breathing modes in DNA, RNA bases
853	$v(C-C)$ collagen proline
872	$v(C-C)$ Collagen hydroxyproline
937	$v(C-C)$ Proline and protein backbone
959-962	$v_1 PO_4^{3-}$
1003	$v(C-C)$ Phenylalanine
1035	$v_3 PO_4^{3-}$ overlaps with proline components
1048	$v_3 PO_4^{3-}$
1060	Proteoglycan
1070	$v_1 CO_3^{2-}$
1076	$v_3 PO_4^{3-}$
1129	$v(C-C)$
1176	$v(C-O-C)$, Tyrosine, Phenylalanine
1204	$\omega(CH_2)$ Tyrosine, hydroxyproline
1242	Amide III, protein β-sheet and random coils
1248	NH_2 Guanine, Cytosine DNA, RNA
1272	Amide III, protein α-helix
1293-1305	$\delta(=CH)$
1320	CH deformations, proteins
1340	Amide III, protein α-helix
1365	Pentosidine
1375	Proteoglycan
1446	$\delta(=CH_2)$
1585	$v(C-C-H)$
1602	Phenylalanine
1609	$\delta(C=C)$, Phenylalanine, tyrosine
1660	Amide I strongest amide I
1690	Amide I

Table 1. Peak position and assignment of major Raman bands observed in osteo-differentiated MSCs and MG-63 cells. References [28, 29].

5

Raman hyperspectral chemical maps, known as chemigrams, were performed in order to have intrinsic biochemical information. Raman chemigrams provide information about the chemical composition. In Raman chemigrams, by selecting specific wavelengths, Raman imaging allows different graphical results to be achieved for the maps of the different cells under investigation. One basic advantage of Raman chemigrams is to localize the Raman spectra to specific areas in the cells.

A   B   C   D

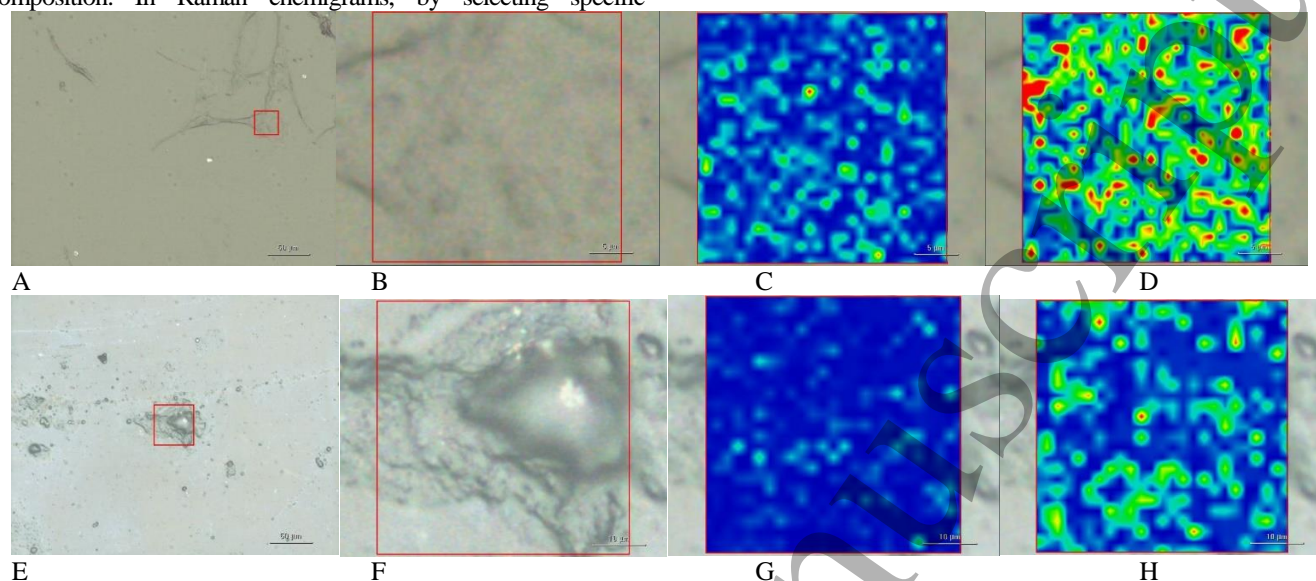E   F   G   H

Figure 4. Raman chemical maps of a MG-63 cell (A-D) and an osteo-differentiated MSC (E-H). The images A and E represent the cells with the red box denoting the area under Raman investigation for MG-63 cell (A) and osteo-differentiated MSC (E), respectively. The images B and F are the correspondent zoomed red box of A and E, respectively. The images C and G are the distribution of cysteine ($668 cm^{-1}$) for MG-63 and osteo-differentiated MSC, respectively. Analogously, the images D and H are the correspondent distribution of HA ($960 cm^{-1}$). The images were collected making use of 50X magnification. Under the experimental setup, the Raman imaging allows the spatial spectroscopy of single cells regions with steps of nearly 1μm.

Raman hyperspectral maps represented in Figure 4 show quite explicitly that the amount of cysteine and HA is decisively higher in MG-63cells because the red regions represent high density of compound and blue regions scarcity of the same substance.

Raman maps displayed in Figure 4 represent an immediate visualization of the results already extracted with the multivariate analysis and confirm that the MG-63 cells contain a higher content of HA and cysteine.

This study was performed on the basis of cells instead of tissues, because Raman spectroscopy can enable subcellular resolution by providing useful information on the molecular composition of cells. However, there are some limitations in biomedicine for example, if we wish to apply Raman spectroscopy to live tissues, the scattering efficiency is generally low. This can require acquisition time of tens of seconds for a single spot, hence, several hours may be needed for tissue areas as required in clinical needs. For this reason, we have tried to improve the Raman signal employing a more powerful optical technique such as SERS. Indeed, SERS can amplify weak Raman signal by providing sample information in a much shorter time frame with improved sensitivity and accuracy than those obtained only via Raman.

In this study, we are also interested in understanding if and how AuNS-based SERS effect can help for probing osteosarcoma differentiation. For cellular and subcellular analysis with SERS, AuNSs were uptaken by the cells [31]. Since the AuNSs optical properties are defined by the plasmons, which are collective oscillations of the conduction electrons. AuNSs efficiently scatter visible or near-infrared light and do not blink or photobleach.

SERS measurements were performed by focusing the laser beam onto the AuNSs, as shown in Figure 5. One limitation of such technique is that, using the same laser excitation, any Raman spectral data would not have been collected from a control cell without AuNSs. Only nearly half spots with AuNSs yielded an SERS spectrum. This is a direct consequence of the fact that the SERS spectrum magnification is observed from molecules that are adsorbed at a specific site of AuNSs where the signal is amplified by AuNSs plasmon resonance.
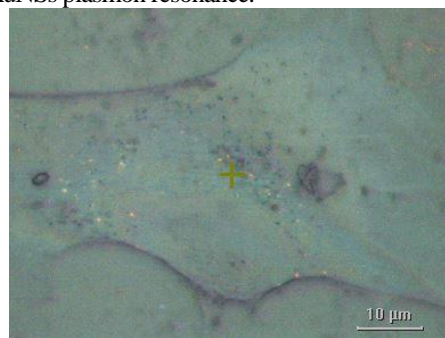

Figure 5. Brightfield illumination at 100X magnification on the DXR Raman microscope of MG-63 cell crowded by AuNSs.

SERS spectra from AuNSs or silver NPs in biological cells include a complicate texture of vibration bands and a rather variability from particle to particle spot. The vibrational modes of SERS spectra can differ due to uncontrolled enhancement factor of biomolecules as a function of the proximity of such biomolecules (proteins, lipids,

DNA and RNA) to AuNSs. Consequently, the assignation can follow Table I, but it may need a supplementary work taking into account specific literature on osteosarcoma [32].
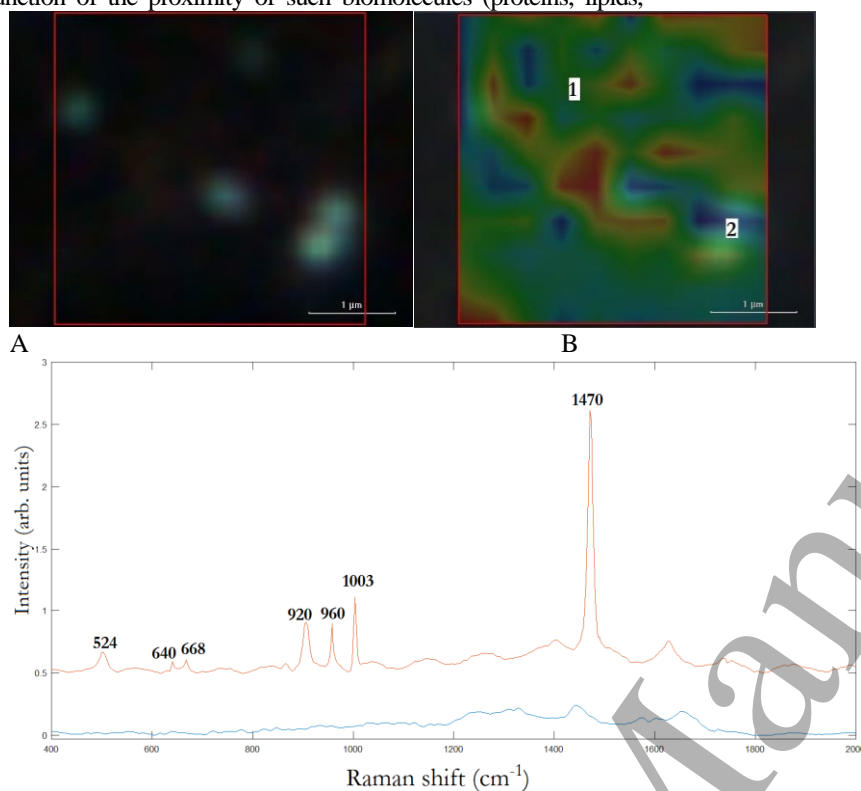

Figure 6. Raman signal from AuNSs. Localization of single AuNSs inside a MG-63 cell, A. Correspondent Raman chemical map , B, where position of AuNSs is denoted by brighter spots. C, Raman spectra of the spots denoted as (1) and (2) in B. With a100X magnification, the laser spot diameter is approximately 700nm.

Figure 6 reports the SERS results on a MG-63 cell and denotes the relative position of the internalized AuNSs inside the red box. Two AuNSs are relatively close one each other thus forming a dimer where the SERS signal is maximum due to the enhancement of the electromagnetic field generated by the relative confinement of the AuNSs. Figure 6B shows Raman chemical map. The brighter spots denotes the AuNSs positions. The spots (1) and (2) correspond to a point unaffected by SERS and to a dimer (maximum SERS signal), respectively. Figure 6 refers the Raman spectra correspondent to spots (1), blue line, and (2), red line, respectively, as in Figure 6B. With respect to the purchase spectrum in point 1, at point 2 we note the enhancement of the Raman signal at the wavevectors corresponding to $524 cm^{-1}$ (corresponding to *S-S* disulfide stretching in proteins), $640 cm^{-1}$ (corresponding both to *C-S* stretching and to *C-C* twisting mode of tyrosine, [28]). In addition, we have the Cysteine peak $668 cm^{-1}$, a peak at $920 cm^{-1}$ corresponding to *C-C* stretch of proline ring [29], HA peak $960 cm^{-1}$, Phe peak $1003 cm^{-1}$; finally the peak at $1470 cm^{-1}$ corresponding to *C=N* stretching [28]. Although SERS improved locally the Raman signals, presenting a good reproducibility and accuracy of SERS, one limitation of our approach is that the SERS signals were generated *in situ*, i.e., by the

dimers, or trimers of AuNSs incorporated in the cells. This *in situ* SERS approach could be limited by the AuNSs dispersion. One of our future developments will be to study the most efficient strategy to have a better SERS signal. Analogously, another future development will be to study the best conditions for the application of Raman spectroscopy to clinical oncology applications.

4. Conclusions

Conventional biochemical methods widely employed to evaluate the MSC-osteoblast or MSC pre-osteoblast-osteosarcoma differentiation, such as immunostaining or reverse transcription polymerase chain reaction, are time consuming and may require a quite large amount of cells, in special way for immunostaining. In addition, the significance of histological results is limited by inter-observer variability, in particular if the cells fall into intermediate range of maturity making a quantitative assessment difficult.

On the contrary, Raman spectroscopy is a label-free optical technology and recent investigations suggest that Raman spectroscopy can be used as a clinical tool in cancer diagnosis to improve diagnostic accuracy.

In this study, we used Raman spectroscopy to the identification and discrimination of MG-63 cells from osteo-

differentiated MCSs. The identification was focused on characteristic cysteine and HA Raman peaks. The results show unequivocally that the presence of these indicators are much greater in the MG-63 cells. The consequences of these results to improve the diagnostic tools are immediate. Raman imaging microscopy has shown high sensitivity, a direct and quantitative measurement of the mineralization level of cells. Combined with AuNSs and exploiting SERS effect, Raman spectroscopy permits the local evaluation of cells through an amplified signal with a resolution lower than 1μm.

Acknowledgements

References

[1] Gardiner D J, Practical Raman spectroscopy, Springer-Verlag, 1989.
[2] Stock G, Domcke W, 1990 *J. Chem. Phys.* **93,** 5496.
[3] Gough J E, Notingher I, Hench L L, 2004 *J. Biomed. Mater. Res. A*, **68**, 640.
[4] Notingher I, Jell G, Lohbauer U, Salih V, Hench LL, 2004 *J. Cell Biochem*, **92**, 1180.
[5] Patel I S, Premasiri W R, Moir D T, Ziegler L D, 2008 *J. Raman. Spectroscopy*, **39**, 1660.
[6] Gupta K, Kim D H, Ellison D, Smith C, Kundu A, Tuan J, et al., 2010 *Lab Chip* **10**, 2019.
[7] Schlücker S, Surface-Enhanced Raman Spectroscopy: Analytical, Biophysical and Life Science Applications, Wiley-VCH, Weinheim, Germany, 2011
[8] Stöckle R M, Suh Y D, Deckert V, Zenobi R, 2000 *Chem. Phys. Lett.* **318**, 131.
[9] Hartschuh A, Sanchez E J, Xie X S, Novotny L, 2003 *Phys. Rev. Lett.* **90**, 095503.
[10] Tolar J, Nauta A J, Osborn M J, Panoskaltsis Mortari A, McElmurry R T, Bell S, et al, 2007 *Stem Cells*, **25**, 371.
[11] Shimizu T, Ishikawa T, Sigihara E, Miyamoto S, et al, 2010 *Oncogene*, **29**, 5687.
[12] Rubio D, Garcia S, Paz M F, De la Cueva T, Lopez-Fernandez L A, Lloyd A C, et al, 2008, *PloS One*, **3**, e1398.
[13] Clover J, Gowen M., 1994, *Bone*, **15**, 585.
[14] Chiang Y H, Wu S H, Kuo Y C, Chen H F, Chiou A, Lee O K, 2015 *Stem Cell Research & Therapy*, **6**, 81.
[15] Wu Z, Yang W, Liu J, Zhang F, 2017 *OncoTargets and Therapy*, **10**, 5329.
[16] Cuscó R, Guitián F, de Aza S., Artús L, 1998 *J. Eur. Ceramics Soc.*, **18**, 1301.
[17] Mandair G S, Morris M D, 2015 Bonekey Reports, **4**, 620.
[18] Jermyn M, Desroches J, Aubertin K, St-Arnaud K, Madore W, De Montigny J E, Guiot M C, Trudel D, Wilson B, Petrecca K, Leblond F, 2016 *Phys. Med. Biol*. **61**, R370.
[19] Strzelecka-Kiliszek A, Bozycki L, Mebarek S, Buchet R, Pikula S, 2017, *J Inorganic Biochem*, **171**, 100.
[20] Scheller J, Chalaris A, Schmidt-Arras D, Rose-John S, 2011 *Biochimica et Biophysica Acta - Molecular Cell Research*, **1813**, 878.
[21] Xiong Y, Ye A, Wen C, Zhang Y, 2010 *Chinese Optics Letters*, **8**, 1015.
[22] Wang Y, Salehi M, Schütz M, Rudi K, Schlücker S, 2013 *Analyst*, **138**, 1764.
[23] Trombi L, Mattii M, Pacini S, D'Alessandro D, Battolla B, Orciuolo E, Buda G, Fazzi R, Galimberti S, Petrini M, 2008 *J Orthop Res*; **26**, 176.
[24] https://nanocomposix.eu/collections/nanoshells.
[25] Danti S, D'Acunto M, Trombi L, Berrettini S, Pietrabissa A, 2007 *Macromolecular Bioscience*, **7**, 589.
[26] www.thermofisher.com
[27] http://www.mathworks.com
[28] Mosavaghi Z, Rehman S, Rehman I U, 2015 *Appl. Spectr. Rev.* **50**, 46.
[29] Simpson R J, Hammacher A, Smith D K, Matthews J M, Ward L D, 1997 *Protein Science*, **6**, 929.
[30] Kleinerman E K, Current Advances in Osteosarcoma, Springer 2014.
[31] D'Acunto M, 2018 *Materials*, **11**, 882.
[32] Tang H-W, Yang X B, Kirkham J, Smith A, 2007 *Anal. Chem.* **79**, 3646.

Table I

Raman shift (cm^{-1})	Band attribution
430-450	$v_2 PO_4^{3-}$ Strong band
584-590	$v_4 PO_4^{3-}$
668	$v(C-S)$ Cysteine
782	Ring breathing modes in DNA, RNA bases
853	$v(C-C)$ collagen proline
872	$v(C-C)$ Collagen hydroxyproline
937	$v(C-C)$ Proline and protein backbone
959-962	$v_1 PO_4^{3-}$
1003	$v(C-C)$ Phenylalanine
1035	$v_3 PO_4^{3-}$ overlaps with proline components
1048	$v_3 PO_4^{3-}$
1060	Proteoglycan
1070	$v_1 CO_3^{2-}$
1076	$v_3 PO_4^{3-}$
1129	$v(C-C)$
1176	$v(C-O-C)$, Tyrosine, Phenylalanine
1204	$\omega(CH_2)$ Tyrosine, hydroxyproline
1242	Amide III, protein β-sheet and random coils
1248	NH_2 Guanine, Cytosine DNA, RNA
1272	Amide III, protein α-helix
1293-1305	$\delta(=CH)$
1320	CH defomartions, proteins
1340	Amide III, protein α-helix
1365	Pentosidine
1375	Proteoglycan

1446	$\delta\left(=CH_2\right)$
1585	$v\left(C-C-H\right)$
1602	Phenylalanine
1609	$\delta\left(C=C\right)$, Phenylalanine, tyrosine
1660	Amide I strongest amide I
1690	Amide I

Table 1. Peak position and assignment of major Raman bands observed in osteo-differentiated MSCs and MG-63 cells. References [21, 26].